Electronic Supplementary Information

N, S-Containing MOF Derived Dual-Doped Mesoporous Carbon as Highly Effective Oxygen Reduction Reaction Electrocatalyst

Ai-Dong Tan[a], Kai Wan[b], Yi-Fang Wang[a], Zhi-Yong Fu[*a,c], Zhen-Xing Liang[*a]

[a] Key Laboratory on Fuel Cell Technology of Guangdong Province, School of Chemistry and Chemical Engineering, South China University of Technology, Guangzhou 510641, P.R. China.

[b] Department of Materials Engineering, KU Leuven, Leuven 3001, Belgium.

[c] State Key Laboratory of Photocatalysis on Energy and Environment, Fuzhou University, Fuzhou 350002, P.R. China.

*Corresponding authors: E-mail: zyfu@scut.edu.cn (Z.Y. Fu); Tel.: +86 20 87113584, E-mail: zliang@scut.edu.cn (Z.X. Liang).

Fig. S1 A view of a) the building unit and paddle wheel dimer, b) the 2D square-grid-like layer, c) the 3D “pillar-layer” cubic framework in SCUT-12, and d) the topologic structure of the framework.

Fig. S2 PXRD patterns of the as-synthesized a) SCUT-12, b) N-MOF, c) S-MOF, d) precursor and their simulated patterns, e) PXRD pattern of NSMC-900.

Fig. S3 Raman spectra of a) NSMCs, and b) N(S)MC-900.

Fig. S4 Nitrogen ad/desorption isotherms and the corresponding pore size distribution of a, b) N(S)MC-900; and c, d) NSMC-900 and NSMC-900 without acid-leaching.

Fig. S5 TEM images of (a) NMC-900, and (b) SMC-900.

Fig. S6 XPS survey spectra of a) NSMC-800, b) NSMC-900, c) NSMC-1000, d) NMC-900, and e) SMC-900.

Fig. S7 a) N 1s peak and the peak fitting result of NMC-900, b) S 2p peak and the peak fitting result of SMC-900.

Fig. S8 C 1s peak and the peak fitting results of a) NSMC-800, b) NSMC-900, c) NSMC-1000, d) NMC-900, and e) SMC-900.

Fig. S9 The plot of C-N/C-S fraction and the current density at 0.90 V of NSMCs *vs*. pyrolysis temperature.

Fig. S10 Electron transfer number obtained by the RRDE results under rotating speeds of 1600 rpm in O_2-saturated 0.10 M KOH: a) NSMCs, and b) N(S)MC-900.

Fig. S11 ORR polarization curves of NSMC-900 and NSC-MOF at a scan rate of 5 mV s^{-1} under rotating speeds of 1600 rpm in O_2-saturated 0.10 M KOH.

Table S1 Crystal data and structure refinement for SCUT-12.

Table S2 Selected bond lengths (Å) and angles (°) for SCUT-12.

Table S3 Pore features of as-synthesized carbon.

Table S4 The content of the carbon components (at. %) of the as-synthesized carbon.

Table S5 Comparison of the ORR performance of typical N, S-codoped carbon catalysts.

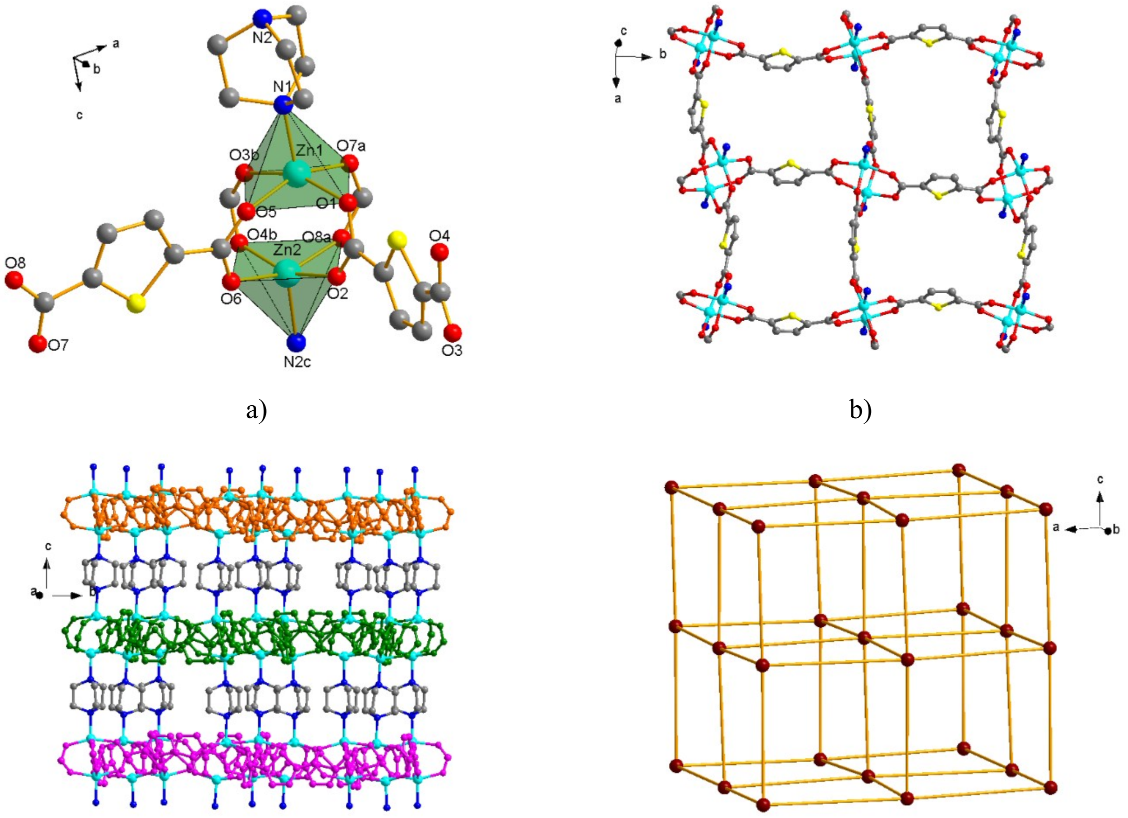

a)

b)

c)

d)

Fig. S1 A view of a) the building unit and paddle wheel dimer, b) the 2D square-grid-like layer, c) the 3D “pillar-layer” cubic framework in SCUT-12, and d) the topologic structure of the framework.

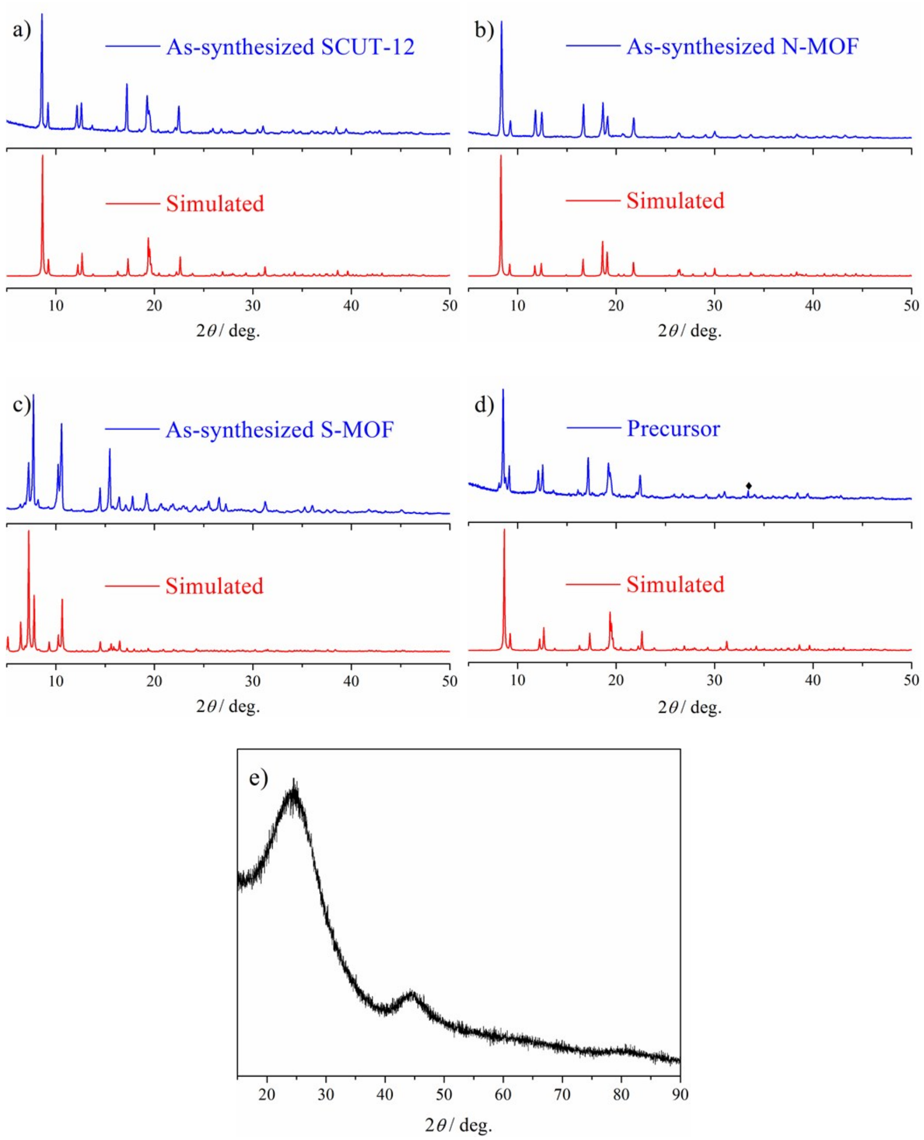

Fig. S2 PXRD patterns of the as-synthesized a) SCUT-12, b) N-MOF, c) S-MOF, d) precursor and their simulated patterns; e) PXRD pattern of NSMC-900.

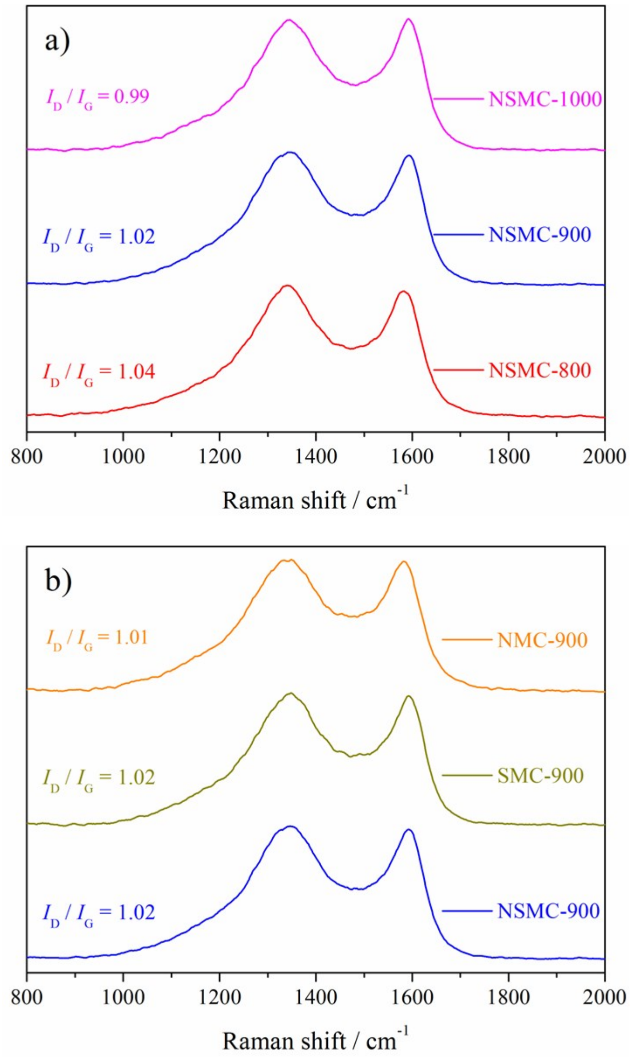

Fig. S3 Raman spectra of a) NSMCs, and b) N(S)MC-900.

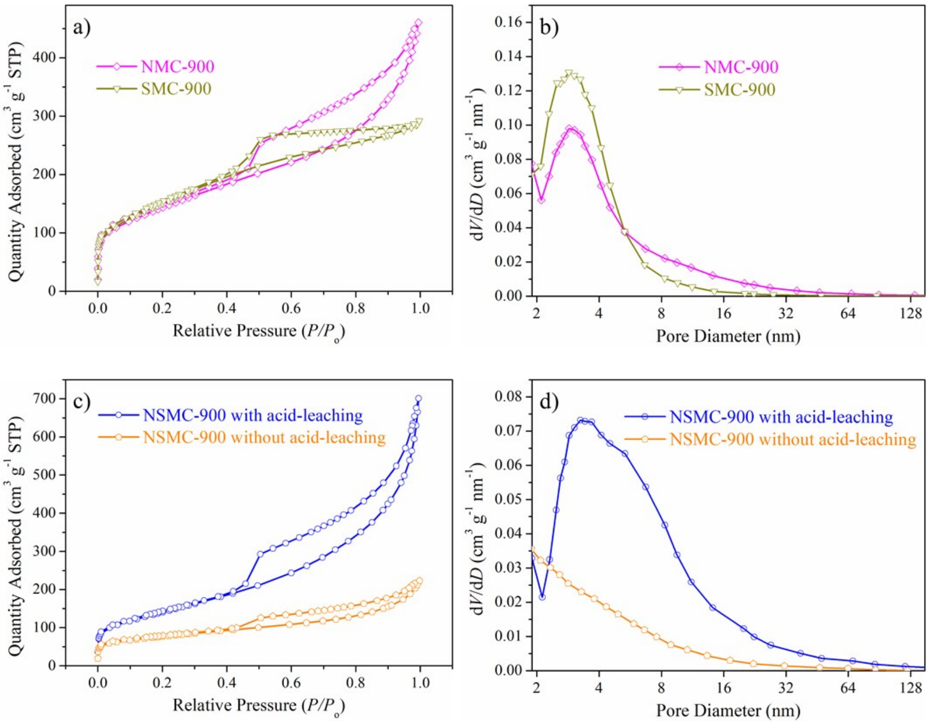

Fig. S4 Nitrogen ad/desorption isotherms and the corresponding pore size distribution of a, b) N(S)MC-900; and c, d) NSMC-900 and NSMC-900 without acid-leaching.

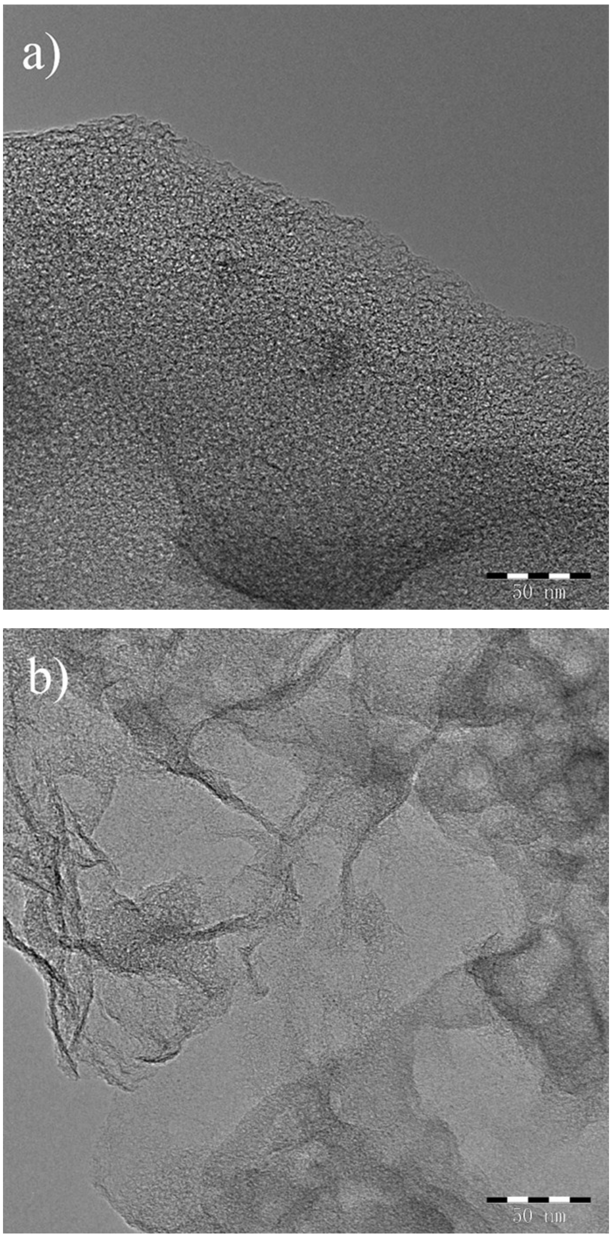

Fig. S5 TEM images of (a) NMC-900, and (b) SMC-900.

It is seen that enriched mesopores with diameter <10 nm are uniformly and compactly distributed in the two carbons, which show much narrower mesopore size distributions than does NSMC (see Figure 2 in manuscript).

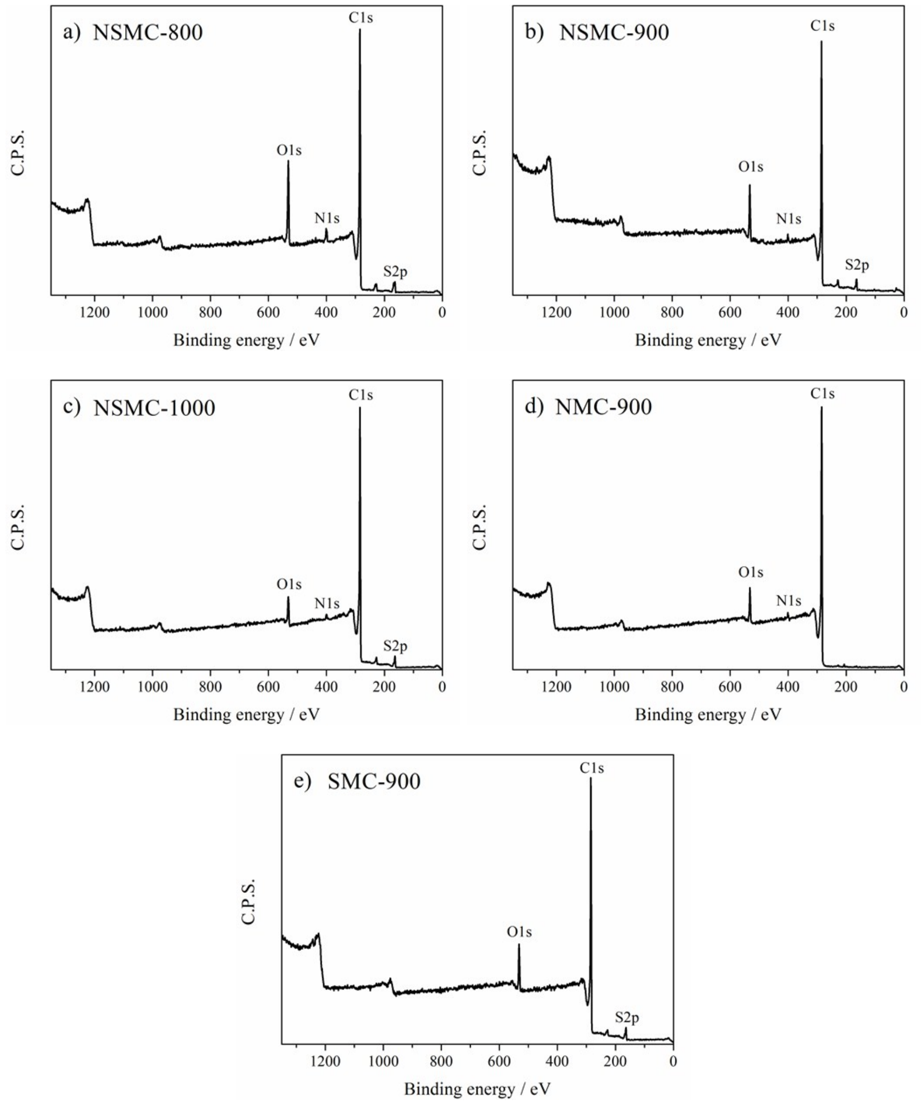

Fig. S6 XPS survey spectra of a) NSMC-800, b) NSMC-900, c) NSMC-1000, d) NMC-900, and e) SMC-900.

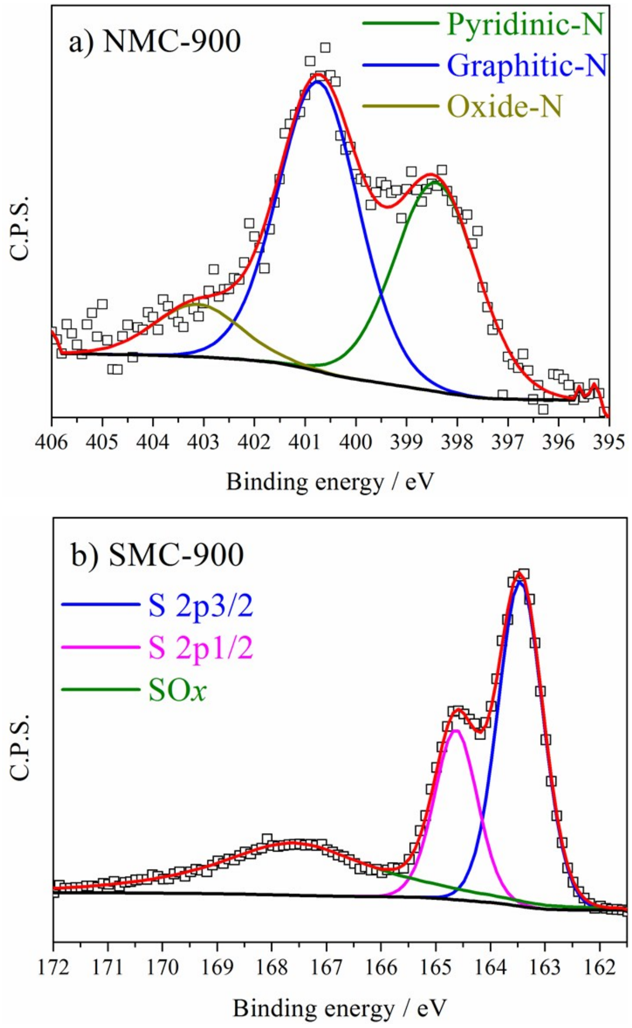

Fig. S7 a) N 1s peak and the peak fitting result of NMC-900; b) S 2p peak and the peak fitting result of SMC-900.

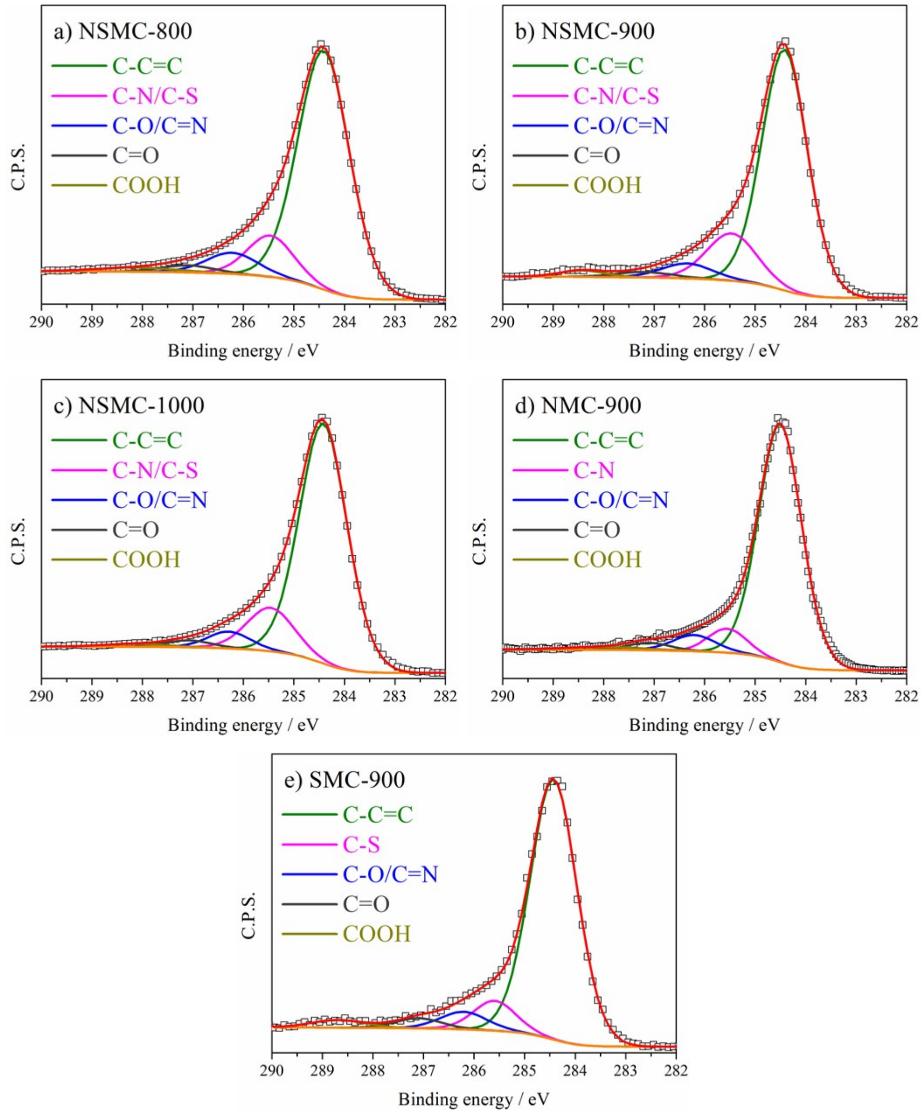

Fig. S8 C 1s peak and the peak fitting results of a) NSMC-800, b) NSMC-900, c) NSMC-1000, d) NMC-900, and e) SMC-900.

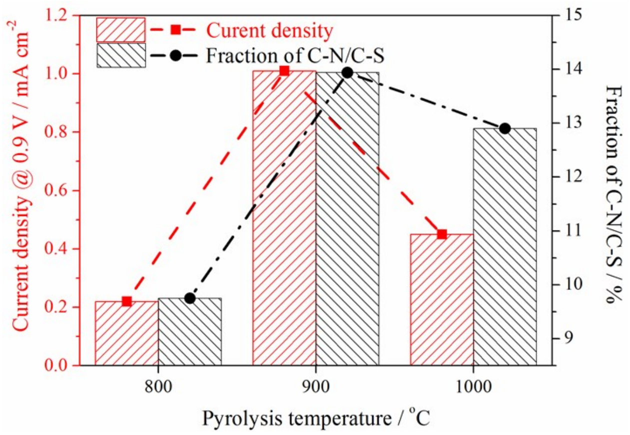

Fig. S9 The plot of C-N/C-S fraction and the current density at 0.90 V of NSMCs *vs*. pyrolysis temperature.

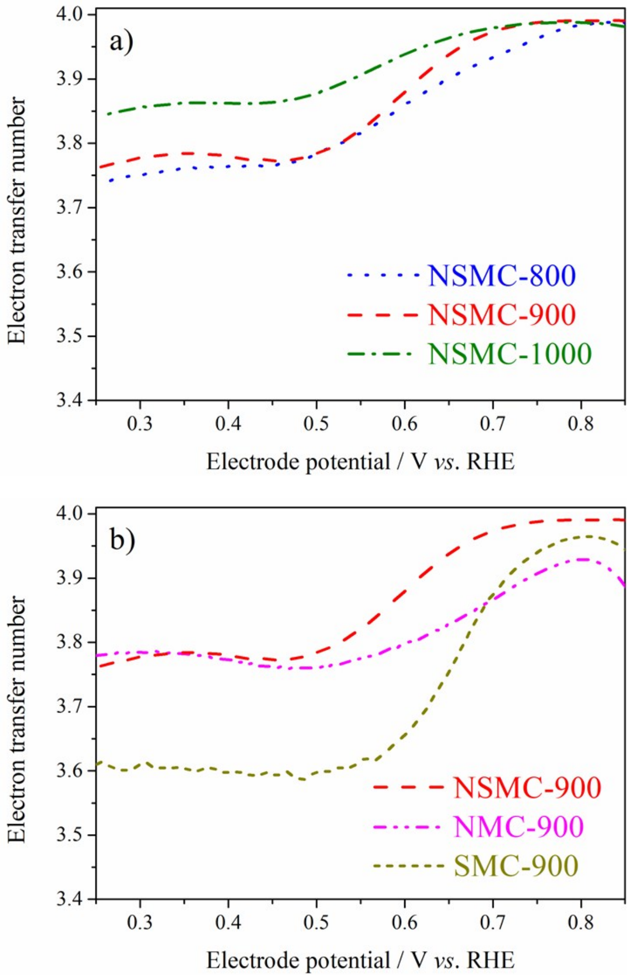

Fig. S10 Electron transfer number obtained by the RRDE results under rotating speeds of 1600 rpm in O_2-saturated 0.10 M KOH: a) NSMCs, and b) N(S)MC-900.

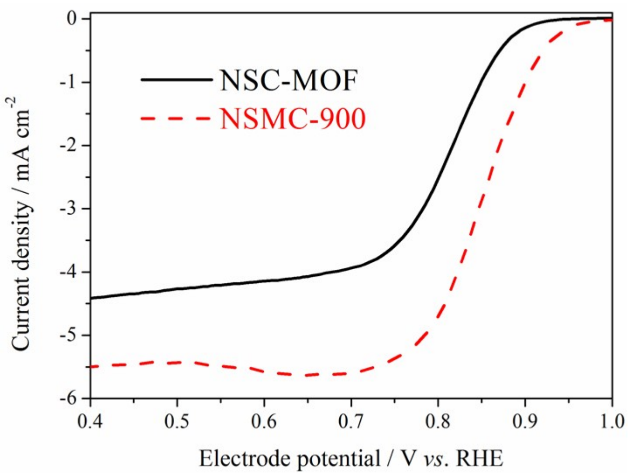

Fig. S11 ORR polarization curves of NSMC-900 and NSC-MOF at a scan rate of 5 mV s^{-1} under rotating speeds of 1600 rpm in O_2-saturated 0.10 M KOH.

The NSC-MOF was prepared by merely using SCUT-12 as a precursor to clarify the role of Fe. It is found that NSC-MOF exhibits a much lower ORR's performance than does the NSMC-900, indicating that Fe, as an essential catalyst, benefits the formation of active sites during pyrolysis, as suggested in our previous work.[S1]

Table S1 Crystal data and structure refinement for SCUT-12.

Compound	CCDC-1571241
Empirical formula	$C_{30}H_{44}N_6O_{12}S_2Zn_2$
Formula weight	875.57
T (K), λ(Mo–Kα) (Å)	173.0(1), 0.71073
Crystal system, space group	Tetragonal, P-42_1c
Unit cell dimensions (Å, °)	$a = 20.469(1)$, $\alpha = 90.0$ $b = 20.469(1)$, $\beta = 90.0$ $c = 19.147(1)$, $\gamma = 90.0$
Volume (Å^3), Z, ρ (g·cm^{-3})	8022.3(2), 8, 1.45
μ (mm^{-1}), F(000)	1.363, 3632
Crystal size (mm)	0.12 × 0.12 × 0.12
θ Range (°)	2.913 - 25.493
Limiting indices	$-24 \leq h \leq 24$, $-17 \leq k \leq 24$, $-23 \leq l \leq 23$
Reflections collected / unique	59996 / 7453
Completeness to $\theta = 25.242$	99.50%
Absorption correction	MUTI-SCAN
Max. and min. transmission	1.00000 - 0.84823
Refinement method	Full-matrix least-squares on F^2
Data / restraints / parameters	7453 / 44 / 478
R_{int}, GOF	0.0431, 1.028
R indices (for obs.): R_1^a, wR_2^b	0.0337, 0.0741
R indices (for all): R_1^a, wR_2^b	0.0388, 0.0768
Largest diff. peak / hole (e.Å^{-3})	0.533 / -0.450

$^aR_1 = \Sigma(||F_o|-|F_c||)/\Sigma|F_o|$, $wR_2 = \{\Sigma w[(F_o^2-F_c^2)^2]/\Sigma w[(F_o^2)^2]\}^{1/2}$;
$^bw = 1/[\sigma^2(F_o^2)+(aP)^2+bP]$, where $P = (F_o^2+2F_c^2)/3]$.

Single crystal of SCUT-12 with appropriate dimensions, 0.12 × 0.12 × 0.12 mm, was chosen under an optical microscope and quickly coated with high vacuum grease (Dow Corning Corporation) before being mounted on a glass fiber for data collection. Data collection for SCUT-12 was performed on a Rigaku Xcalibur Eos Gemini CCD diffractometer. Empirical absorption corrections were applied for SCUT-12 with the MUTI-SCAN program.[S2] The systematic absence analyzed for SCUT-12 by the XPREP program in the SHELXL-2014 software package[S3] suggested P-42_1c (No. 114) as the highest possible space group. The structures were solved by direct methods using SHELXS-2014 and refined on F^2 by full-matrix least-squares techniques using SHELXL-2014. All non-hydrogen atoms were located from iterative examination of difference *F*-maps following least squares refinements of the earlier models and treated anisotropically. The positions of organic hydrogen atoms were generated geometrically. The structure was examined using the Addsym subroutine of PLATON[S4] to assure that no additional symmetry could be applied to the models. Final refinement converged at R_1 = 0.0337 for SCUT-12. More details on crystallographic information have been deposited in the cif format as CCDC-1571241 in the Cambridge Crystallographic Data Centre.

Table S2 Selected bond lengths (Å) and angles (°) for SCUT-12.

Bond Lengths			
Zn(1)-O(1)	2.023(3)	Zn(1)-O(3*b*)	2.058(3)
Zn(1)-O(5)	2.059(3)	Zn(1)-O(7*a*)	2.029(3)
Zn(1)-N(1)	2.046(3)	Zn(2)-O(2)	2.067(3)
Zn(2)-O(4*b*)	2.047(3)	Zn(2)-O(6)	2.027(3)
Zn(2)-O(8*a*)	2.053(3)	Zn(2)-N(2*c*)	2.055(3)
S(1)-C(2)	1.717(5)	S(1)-C(5)	1.715(5)
S(2)-C(11)	1.717(5)	S(2)-C(8)	1.714(5)
Bond Angles			
O(1)-Zn(1)-N(1)	105.1(2)	O(1)-Zn(1)-O(3*b*)	156.8(2)
O(1)-Zn(1)-O(5)	86.0(2)	O(1)-Zn(1)-O(7*a*)	89.5(2)
O(3*b*)-Zn(1)-N(1)	97.6(2)	O(3*b*)-Zn(1)-O(5)	86.4(2)
O(3*b*)-Zn(1)-O(7*a*)	89.1(2)	O(5)-Zn(1)-N(1)	97.9(1)
O(5)-Zn(1)-O(7*a*)	157.1(1)	O(7*a*)-Zn(1)-N(1)	105.0(1)
O(2)-Zn(2)-N(2*c*)	100.1(1)	O(2)-Zn(2)-O(4*b*)	158.5(1)
O(2)-Zn(2)-O(6)	89.7(2)	O(2)-Zn(2)-O(8*a*)	86.4(2)
O(4*b*)-Zn(2)-N(2*c*)	101.1(1)	O(4*b*)-Zn(2)-O(6)	89.2(2)
O(4*b*)-Zn(2)-O(8*a*)	86.7(2)	O(6)-Zn(2)-N(2*c*)	104.0(1)
O(6)-Zn(2)-O(8*a*)	158.0(1)	O(8*a*)-Zn(2)-N(2*c*)	98.1(2)
C(2)-S(1)-C(5)	91.4(2)	C(8)-S(2)-C(11)	91.2(2)

Symmetry transformations used to generate equivalent atoms: *a* x+1/2,-y+1/2,-z+1/2; *b* -x+1/2,y-1/2,-z+1/2; *c* -y+1/2,-x+1/2,z+1/2; *d* x-1/2,-y+1/2,-z+1/2; *e* -x+1/2,y+1/2,-z+1/2; *f* -y+1/2,-x+1/2,z-1/2.

Table S3 Pore features of as-synthesized carbon.

Sample	S_{BET} (m^2 g^{-1})	S_{meso} (m^2 g^{-1})	D_{BJH} (nm)
NSMC-800	452	255	6.3
NSMC-900	499	281	6.7
NSMC-1000	492	287	7.2
NMC-900	508	267	5.4
SMC-900	536	298	3.4
NSMC-900*	268	61	5.6

(*without acid-leaching)

Table S4 The content of the carbon components (at. %) of the as-synthesized carbon.

Sample	C-C=C	C-N/C-S	C-O/C=N	C=O	COOH
NSMC-800	76.87	11.97	6.81	2.27	2.08
NSMC-900	74.58	16.16	5.18	2.10	1.98
NSMC-1000	77.59	14.06	4.90	2.18	1.27
NMC-900	82.48	7.37	5.70	2.56	1.89
SMC-900	80.38	8.32	5.82	3.12	2.36

(The binding energy of each type carbon is 284.4, 285.4, 286.3, 287.2 and 288.2 ± 0.2 eV. The full-width at half-maximum is set to be 1.1 ± 0.2 eV except for COOH.)

Table S5 Comparison of the ORR performance of typical N, S-codoped carbon catalysts.

Catalyst	E_{onset} *vs* RHE (V)	$E_{1/2}$ *vs* RHE (V)	Content of N and S (at. %)	Ref.
NSMC-900	0.98	0.85	2.19, 2.91	This work
N,S-NH_3-C-7	0.97	0.84	5.40, 0.30	S5
ZIF-TAA-p	0.98	0.88	6.69, 0.41	S6
NS(3:1)-C-MOF-5	0.96	--	3.31, 1.08	S7
SN-OMC	0.97	--	3.4, 5.06	S8
Fe-SNC	0.98	0.84	1.87, 0.70	S9
N/S-2DPC-60	0.86	--	5.39, 0.26 wt.%	S10
1100-CNS	0.99	0.85	1.33, 1.88 wt.%	S11
N,S-PGN-700	0.93	0.82	12.50, 1.90	S12
N_1S_1-CNW-900	0.91	0.84	3.57, 1.15	S13
N-S-HPC	0.99	0.86	3.90, 0.76	S14

Reference

S1 A. D. Tan, Y. F. Wang, Z. Y. Fu, P. Tsiakaras, Z. X. Liang, *Appl. Catal. B-Environ.*, 2017, **218**, 260-266.

S2 Rigaku, CrysAlisPro 1.171.38.41, Rigaku Corporation, Tokyo, Japan, 2015.

S3 G. M. Sheldrick, *Acta Crystallogr.*, 2008, **A64**, 112-122.

S4 A. L. Spek, Implemented as the PLATON procedure, a multipurpose crystallographic tool, Utrecht University, Ultrecht, The Netherlands, 1998.

S5 Z. Song, W. Liu, N. Cheng, M. Norouzi Banis, X. Li, Q. Sun, B. Xiao, Y. Liu, A. Lushington, R. Li, L. Liu, X. Sun, *Mater. Horiz.*, 2017, **4**, 900-907..

S6 C. Zhang, B. An, L. Yang, B. B. Wu, W. Shi, Y. C. Wang, L.S. Long, C. Wang, W. B. Lin, *J. Mater. Chem. A*, 2016, **4**, 4457-4463.

S7 J. S. Li, Y. Y. Chen, Y. J. Tang, S. L. Li, H. Q. Dong, K. Li, M. Han, Y. Q. Lan, J. C. Bao, Z. H. Dai, *J. Mater. Chem. A*, 2014, **2**, 6316-6319.

S8 Y. Q. Hua, T. T. Jiang, K. Wang, M. M. Wu, S. Q. Song, Y. Wang, P. Tsiakaras, *Appl. Catal. B-Environ.*, 2016, **194**, 202-208.

S9 M. H. Naveen, K. Shim, M. S. A. Hossain, J. H. Kim, Y. B. Shim, *Adv. Energy. Mater.*, 2017, **7**, 1602002-1602002.

S10 Y. Z. Su, Z. Q. Yao, F. Zhang, H. Wang, Z. Mics, E. Canovas, M. Bonn, X. D. Zhuang, X. L. Feng, *Adv. Funct. Mater.*, 2016, **26**, 5893-5902.

S11 Z. X. Pei, H. F. Li, Y. Huang, Q. Xue, Y. Huang, M. S. Zhu, Z. F. Wang, C. Y. Zhi, *Energ. Environ. Sci.*, 2017, **10**, 742-749.

S12 M. Wu, Y. Liu, Y. Zhu, J. Lin, J. Liu, H. Hu, Y. Wang, Q. Zhao, R. Lv, J. Qiu, *J. Mater.*

Chem. A, 2017, **5**, 11331-11339.

S13 S. F. Fu, C. Z. Zhu, J. H. Song, M. H. Engelhard, X. L. Li, P. N. Zhang, H. B. Xia, D. Du, Y. H. Lin, *Nano Res.*, 2017, **10**, 1888-1895.

S14 M. Wu, J. Qiao, K. Li, X. Zhou, Y. Liu, J. Zhang, *Green Chem.*, 2016, **18**, 2699-2709.